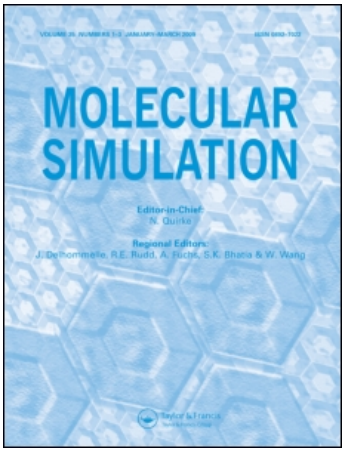

Molecular Simulation
Publication details, including instructions for authors and subscription information:
http://www.informaworld.com/smpp/title~content=t713644482

Multiscale modelling of asphaltene disaggregation

Stanislav R. Stoyanov[ab]; Sergey Gusarov[a]; Andriy Kovalenko[a]
[a] National Institute for Nanotechnology, National Research Council of Canada, Edmonton, AB, Canada
[b] Department of Mechanical Engineering, University of Alberta, Edmonton, AB, Canada

To cite this Article Stoyanov, Stanislav R. , Gusarov, Sergey and Kovalenko, Andriy(2008) 'Multiscale modelling of asphaltene disaggregation', Molecular Simulation, 34: 10, 953 — 960
To link to this Article: DOI: 10.1080/08927020802411711
URL: http://dx.doi.org/10.1080/08927020802411711

Molecular Simulation
Vol. 34, Nos. 10–15, September–December 2008, 953–960

Taylor & Francis
Taylor & Francis Group

Multiscale modelling of asphaltene disaggregation

Stanislav R. Stoyanov[ab], Sergey Gusarov[a] and Andriy Kovalenko[ab]*

[a]*National Institute for Nanotechnology, National Research Council of Canada, Edmonton, AB, Canada T6G 2M9;* [b]*Department of Mechanical Engineering, University of Alberta, Edmonton, AB, Canada T6G 2G8*

(*Received 31 January 2008; final version received 12 August 2008*)

Asphaltene aggregation reduces bitumen upgrading efficiency by increasing bitumen viscosity and coke formation. Our approach to model asphaltene aggregation involves geometry optimisation by using the Harris approximation implemented in DMol^3, followed by a solvation calculation by using the three-dimensional molecular theory of solvation (a.k.a. 3D-RISM) we have developed recently [A. Kovalenko, *Three-dimensional RISM theory for molecular liquids and solid–liquid interfaces*, in *Understanding Chemical Reactivity: Molecular Theory of Solvation*, F. Hirata ed., Vol. 24, Kluwer Academic Publishers, New York, NY, 2003, pp. 169–275]. From the Harris approximation, we obtain the Hirshfeld and Mulliken asphaltene atomic charges. The 3D-RISM theory allows one to model solvation at given temperature, solvent density and solvent composition. The theory predicts solvation structure and thermodynamic characteristics, such as the potential of mean force (PMF). We investigate the effect of the Hirshfeld and Mulliken charge calculation methods on the PMF values for asphaltene disaggregation in quinoline and 1-methylnaphthalene solvents at 298 and 473 K. Our PMF results predict that asphaltene disaggregation is favoured in quinoline at 473 K, whereas in 1-methylnaphthalene the asphaltene aggregate would remain undisturbed. These results are in agreement with the experiment and correlate with the molecular dynamics (MD) simulation results [T. Takanohashi, S. Sato, and R. Tanaka, *Structural relaxation behaviors of three different asphaltenes using MD calculations*, Petr. Sci. Technol. 22 (2004), pp. 901–904]. The statistical–mechanical 3D-RISM method probes the entire phase space and yields the solvation structure and thermodynamics at a much lower computational cost than MD, and thus gives access to solvation processes that occur on large time and space scales.

Keywords: bitumen; asphaltene disaggregation; potential of mean force; molecular theory of solvation; 3D-RISM

1. Introduction

Bitumen is a mixture of immature and complex hydrocarbons with a relatively low hydrogen-to-carbon ratio (i.e. very aromatic) and an abundance of chemical impurities [1]. Bitumen contains polar (asphaltenes) and non-polar hydrocarbons (maltenes). The asphaltene molecules form stable aggregates that are difficult to characterise at molecular level. Molecular simulations techniques have been applied for estimating the molecular-level interactions in asphaltenes. Computational modelling has shown that asphaltene aggregates are the most stable conformations [2–4]. Molecular dynamics (MD) and molecular mechanics simulations of Khafji asphaltene show that asphaltene aggregates stabilised by $\pi-\pi$ bonding exist even at 673 K and might become coke precursors [5]. The MD simulations of Khafji and Maya asphaltenes show that soaking in quinoline disrupts some stacking interactions, whereas soaking in 1-methylnaphthalene does not cause disaggregation, both in agreement with the experiment [6,7]. The MD modelling results for other asphaltenes indicate that the solvent and heat-treatment effects on disaggregation could be asphaltene specific [7]. These results suggest that asphaltene disaggregation modelling in solution under high temperature requires fast and efficient probing of many structures, solvent systems, temperatures, pressures and time scales.

Bitumen hydrotreatment tests in *critical conditions* show superior performance with reduced zeolite coking and enhanced transport of hydrogen reactant to the catalyst surface, which promotes the desired reaction pathways [8]. For modelling of the processes in *critical conditions*, our group has implemented the three-dimensional molecular theory of solvation, or three-dimensional reference interaction site model (3D-RISM) theory [9], in the ADF quantum chemistry software package [10,11]. The coupling of the Kohn–Sham density functional theory (KS-DFT) with the 3D-RISM integral equation formalism with the Kovalenko–Hirata (KH) closure [12] allows one to model chemical reactions in solution described by NVT ensemble (N = number of particles, V = volume, T = temperature). The KH closure reproduces vapour–liquid phase diagrams and structure in gas as well as liquid phases [13,14]. Another promising task is the modelling of chemical reaction control by using external electric field. Nanoscale control of ion adsorption and desorption using homogenous electric fields has been

*Corresponding author. Email: andriy.kovalenko@nrc-cnrc.gc.ca

ISSN 0892-7022 print/ISSN 1029-0435 online

DOI: 10.1080/08927020802411711
http://www.informaworld.com

demonstrated by us [15]. This idea can be extended to catalytic control of chemical reactions, including bitumen upgrading on zeolite surfaces. We have recently presented a multiscale investigation of zeolite nanoparticle acidity, in particular zeolite surface acidity, and have shown that Fukui functions can be applied for nanoparticle reactivity prediction. The Fukui function maps are considered useful for the development of surface reactivity maps that could be applied for the design of nanoparticles with optimal functionality [16].

Here, we show that the Harris approximation and the statistical–mechanical 3D-RISM theory can be combined to yield a fast and highly effective method for modelling of bitumen upgrading in *critical conditions*. This is part of a project developing a methodology for nanoparticle reactivity prediction that would allow one to probe many catalytic structures in a wide range of external conditions.

2. Computational technique

The starting aggregate geometry of Maya asphaltene is obtained from the MD simulation studies of Takanohashi et al. [7]. This structure is subsequently optimised by using the density functional theory (DFT) Harris approximation, implemented in the DMol^3 software from the Accelrys Materials Studio® 4.0 commercial software package [17]. The Harris approximation [18] calculation is performed by using the local density approximation and the Vosko, Wilk and Nusair functional [19]. In the Harris approximation, the density from the first SCF iteration is used to compute the energy and forces on the atoms. This density, composed of the superimposed charge density from isolated atoms, is a remarkably good approximation when reasonable geometries are needed [17]. We selected the Harris approximation because it allows for the calculation of atomic charges at low computational cost. For the Harris approximation calculation, we use the all-electron double numerical basis set (DN) [20]. The electronic singlet states were treated using single determinants. The real space cut-off for the atomic numerical basis set calculation was set to 4.0 Å. The geometry optimisation convergence was achieved when the energy, gradient and displacement were lower than 1×10^{-5} Ha, 1×10^{-3} Ha/Å and 1×10^{-3} Å, respectively.

The solvent atomic charges needed for the 3D-RISM modelling are calculated for the optimised geometries. The solute atomic charges are calculated as follows. First, the geometry of the entire aggregate is optimised (Figure 1). Second, single-point calculations are performed separately for each of the molecules **a**, **bc** and **d**. This approach ensures that total charge of each molecule is zero. For comparison, we calculate another set of solute atomic charges by single-point calculation for the entire aggregate **abcd** at each solute disaggregation geometry, and refer to it as single point for entire aggregate. The atomic charges are calculated using the Hirshfeld and Mulliken population analysis methods. The Hirshfeld partitioned atomic charges are defined relative to the deformation density, which is the difference between the molecular and the unrelaxed atomic charge densities [21]. In the Mulliken population analysis, the electrons are first divided among all basis functions. The partial atomic charges are defined as the difference between the atomic number and the gross atomic population, which is defined as the sum of the gross orbital populations of all basis functions on a given atom [22].

The solvent thermodynamics and distribution are calculated using the 1D-RISM theory. The number of grid points is 16,384 and the spacing between them is 0.025 Å. The boiling points of quinoline and 1-methylnaphthalene are 511 and 491 K, respectively. The solvent densities at 473 K are taken just above the densities, at which the 1D-RISM theory predicts solvent phase transition. The 1D-RISM solvent distribution file convergence is achieved for quinoline number density of 5.256×10^{-3} and 4.581×10^{-3} Å at 298 and 473 K, respectively. For 1-methylnaphthalene, the number density values used are 4.477×10^{-3} and 4.117×10^{-3} Å at 298 and 473 K, respectively.

The 3D-RISM theory is described elsewhere [9–12]. In this calculation, each solvent and solute atom is modelled explicitly. The potential parameters $\sigma_C = 3.80$ Å, $\sigma_N = 3.90$ Å, $\sigma_O = 3.60$ Å, $\sigma_{H(on\ C)} = 2.60$ Å, $\sigma_{H(on\ O)} = 1.30$ Å, $\varepsilon_C = 0.08$ kcal/mol, $\varepsilon_N = 0.20$ kcal/mol, $\varepsilon_O = 0.15$ kcal/mol, $\varepsilon_{H(on\ C)} = 0.008$ kcal/mol and $\varepsilon_{H(on\ O)} = 0.10$ kcal/mol are from Freindorf et al. [23]. The potential parameters $\sigma_s = 3.550$ Å and $\varepsilon_S = 0.250$ kcal/mol are from Jorgensen and Tirado-Rives [24]. The 3D-RISM/KH equations are solved on a grid of 128^3 points in a cubic supercell of size 64 Å with ambient solvent temperature of 298 and 473 K. Our convergence tests have shown that for a grid of 256^3 points and the same supercell size, the potential of mean force (PMF) values decrease by ~0.2 kcal/mol.

3. Discussion

In Figure 1, we show the Maya asphaltene aggregate that contains three molecules labelled as **a**, **bc** and **d**. Molecules **a** and **d** contain one continuous heterocyclic conjugated system each, whereas **bc** contains two continuous conjugated heterocyclic systems that are tethered by an aliphatic hydrocarbon chain. Asphaltene aggregates are stabilised by van der Waals, electrostatic and π–π interaction forces. The Maya asphaltene aggregation energy E_{AG}, calculated relative to the three non-optimised asphaltene molecules, obtained from the Harris approximation is −35 kcal/mol ($E_{AG} = E_{abcd} - E_a - E_{bc} - E_d$). Alvarez-Ramirez et al. have performed extensive configuration search and calculated a number of asphaltene–asphaltene pair potentials using two DFT methods:

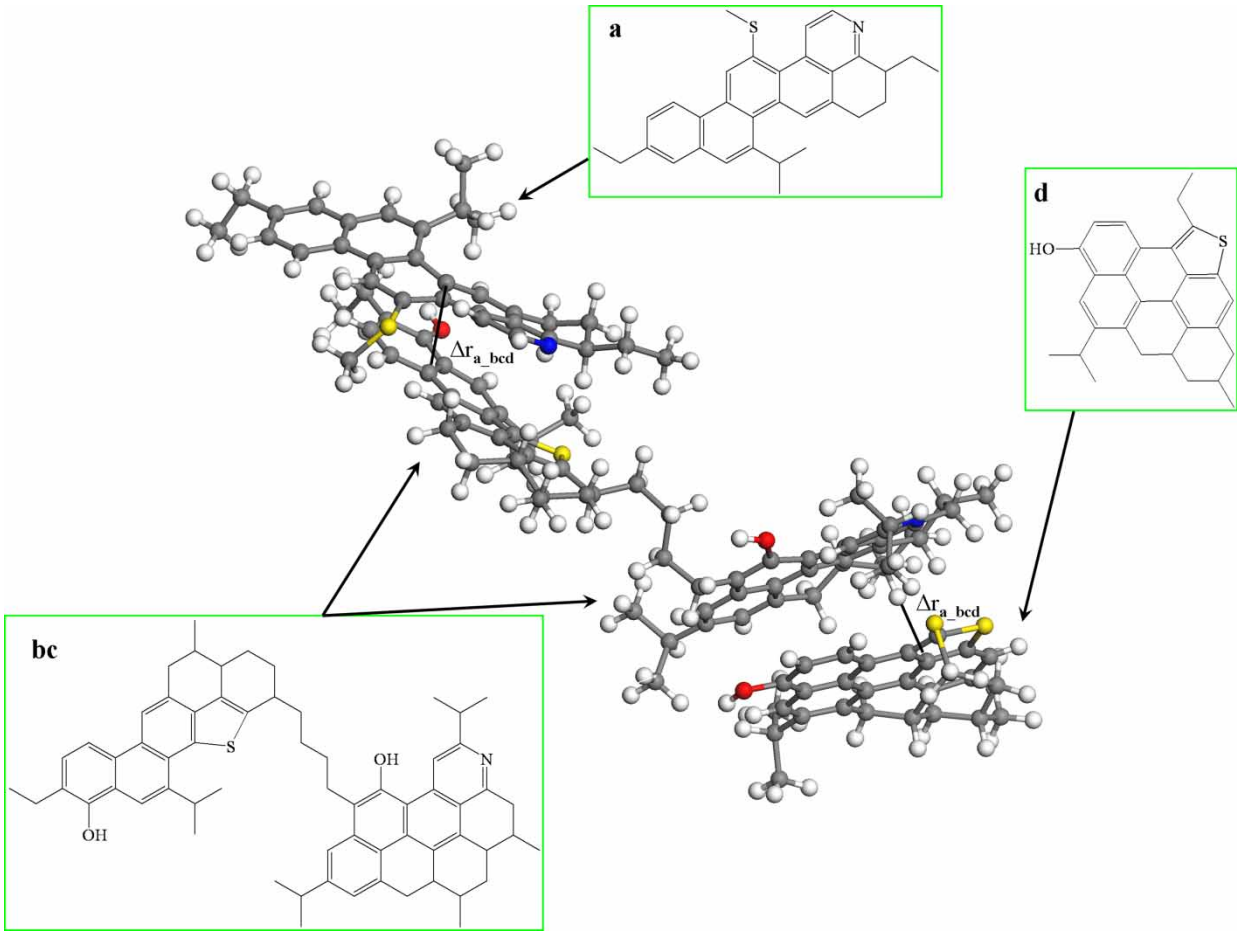

Figure 1. Optimised geometry of Maya asphaltene by using Harris/DN/DMol[3].

Harris approximation and Perdew–Wang exchange-correlation functional (PW91) [25]. These authors obtained E_{AG} values in the range −12 to −15 kcal/mol relative to two non-optimised asphaltene molecules [26]. Considering that Maya asphaltene contains two asphaltene–asphaltene pairs, our E_{AG} value is in reasonable agreement with the latter report.

In Figure 2, we show two disaggregation configurations of Maya asphaltene, considered in this study. The asphaltene disaggregation geometries are prepared by the displacement of molecule **a** while keeping molecules **bc** and **d** fixed, and are abelled as **a_bcd**. In disaggregation configuration I, a set of disaggregation geometries is prepared by the displacement of molecule **a** by 0.25 Å in a direction perpendicular to the best-fit plane defined by all atoms of **a**. The displacement is labelled as $\Delta r^{I}_{a\_bcd}$. In disaggregation configuration II, the geometries are prepared by the displacement of molecule **a** by 0.5 and 0.25 Å in a direction perpendicular and along the best-fit plane, respectively, followed by a rotation of **a** by 2° about the median axis of the best-fit plane of **a**. The displacement is labelled as $\Delta r^{II}_{a\_bcd}$. A disaggregation configuration similar to II

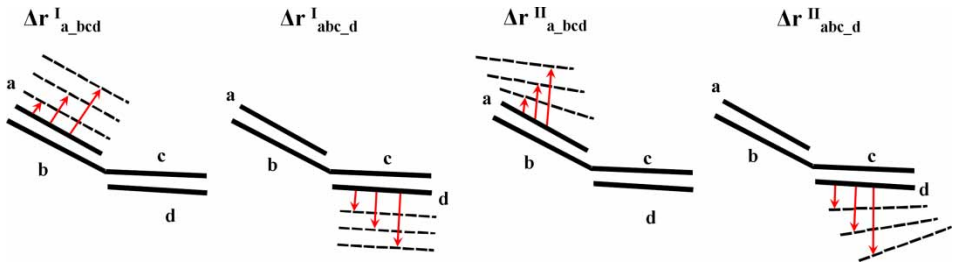

Figure 2. Disaggregation configurations of Maya asphaltene.

has been reported by Takanohashi et al. from the MD simulations in quinoline [7]. Two sets of disaggregation geometries have also been prepared by the displacement of molecule **d** while keeping molecules **a** and **bc** fixed, labelled as $\Delta r^{I}_{abc\_d}$ and $\Delta r^{II}_{abc\_d}$. The interatomic distances that correspond to $\Delta r^{I}_{a\_bcd}$ and $\Delta r^{I}_{abc\_d}$ are shown in Figure 1 as solid lines. For each of these geometries, we apply two sets of atomic charges obtained from the Hirshfeld and Mulliken population analysis methods. For each of these geometries, atomic charge sets, the solvents quinoline and 1-methylnaphthalene, we calculate the PMF at 298 and 473 K using the 3D-RISM theory. In addition, we performed a potential energy disaggregation path search for molecule **a** disaggregation by geometry optimisation with constrained distance Δr_{a_bcd}. The partially optimised geometries for Δr_{a_bcd} of 7.0 and 11.0 Å shown in Figure 3 are qualitatively similar to the MD results of Takanohashi et al. [7]. For each of the partially optimised geometries and the atomic charges obtained from the Hirshfeld population analysis method, we calculate the PMF in the above solvents and temperatures using the 3D-RISM theory.

In Figure 4, we show the dependence of PMF on the distance between the asphaltene molecules. The PMF minima correspond to the most stable aggregation geometry, whereas the maxima correspond to the geometry at which solvent molecules begin entering between the asphaltene aggregates. At distances larger than the latter, the detached asphaltene molecules become solvated. From these plots, we note that the PMF values decrease as the solvent temperature and density are increased. Also, the PMF values in quinoline are higher than 1-methylnaphthalene. Both of these dependencies are related to the respective number density values. By comparing the plots on the left-hand side to those on the right-hand side, we find that the PMF minima for **a_bcd** are higher than those for **abc_d**, whereas the PMF maxima of **a_bcd** are lower than those for **abc_d**. This indicates that the **a_bcd** aggregation is weaker than the **abc_d** one. By comparing the plots obtained using the Hirshfeld atomic charges (top) to those obtained using the Mulliken atomic charges (bottom), we find that the Hirshfeld method derived charges yield PMF with lower minima and higher maxima relative to the Mulliken charges.

In Table 1, we list the PMF minimum and maximum values obtained for the disaggregation configurations I and II. The two main factors that we investigate are the charge calculation methods and the disaggregation configurations. First, we consider the Hirshfeld charges. In quinoline, the $PMF_{max} - PMF_{min}$ values decrease by 2.4 and 5.1 kcal/mol for **a_bcd** and **abc_d** disaggregation, respectively, as the temperature is increased from 298 to 473 K. The lower $PMF_{max} - PMF_{min}$ values in quinoline at 473 relative to 298 K show that Maya asphaltene disaggregation is favoured at high temperature. In 1-methylnaphthalene solvent, the $PMF_{max} - PMF_{min}$ values for **a_bcd** disaggregation increase by $\sim$0.4 kcal/mol as the temperature is increased, indicating that this disaggregation is not favoured by heating. The $PMF_{max} - PMF_{min}$ values for **abc_d** disaggregation change by $\sim$1 kcal/mol upon heating, indicating very small solvent effect on disaggregation. Second, we note that the use of atomic charges obtained from the Mulliken population analysis method yields PMF values that are in qualitative agreement with the Hirshfeld one. The $PMF_{max} - PMF_{min}$ values from Mulliken charges are lower than Hirshfeld, suggesting that preference be given to the use of the Hirshfeld charges. For the two charge calculation methods,

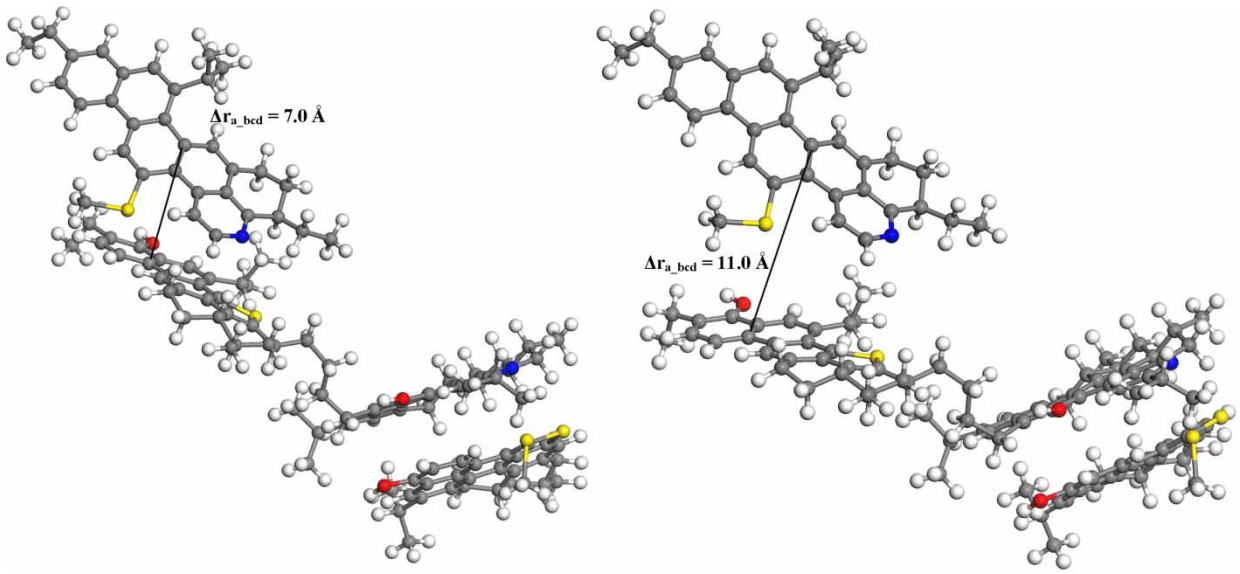

Figure 3. Partially optimised geometry of Maya asphaltene.

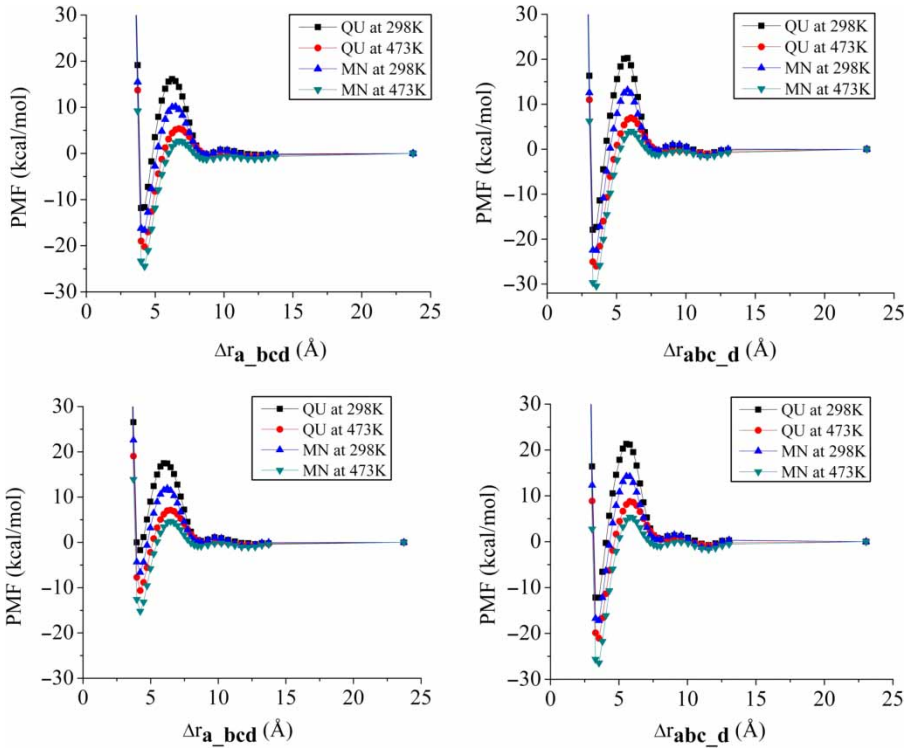

Figure 4. PMF plots for Maya asphaltene disaggregation in quinoline (QU) and 1-methylnaphthalene (MN) at 298 and 473 K in NVT. Charges are obtained from single-point calculations of the entire aggregate by using the Hirshfeld population analysis method (top panels) and Mulliken (bottom panels). Left panels, part a disaggregates; right panels, part b disaggregates. The Maya asphaltene geometry is optimised by using Harris/DN/DMol^3.

the $PMF_{max} - PMF_{min}$ values of **a_bcd** are lower than **abc_d**, suggesting that **a_bcd** is the preferred Maya asphaltene disaggregation configuration. This is in agreement with the more expensive MD simulation results that show preferred disaggregation of molecule **a** [7].

In Table 1, we also list the results obtained from single-point calculation of the entire aggregate by using the Hirshfeld population analysis method. Comparison of the $PMF_{max} - PMF_{min}$ values obtained by this method with the charges for neutral molecules shows that the single-point charge calculation does not lead to significant changes. By computing solute atomic charges using single-point calculation of the entire aggregate we obtain a more accurate but rather expensive description of the evolution of the solute electrostatic potential upon disaggregation.

Disaggregation configuration II yields larger change in the $PMF_{max} - PMF_{min}$ values of **a_bcd** as the temperature is increased relative to configuration I. In quinoline, the $PMF_{max} - PMF_{min}$ values decrease by 3.5 kcal/mol for **a_bcd** disaggregation as the temperature is increased from 298 to 473 K. It is interesting to note that the effect of configuration II on **abc_d** disaggregation is opposite, suggesting that for the latter disaggregation mode I would be more favourable. These results show that it is difficult to predict the preferred asphaltene disaggregation configuration. The strong configuration dependence of the $PMF_{max} - PMF_{min}$ value implies that the actual disaggregation would be even more favoured than the two cases investigated. Our recent experience suggests that asphaltene

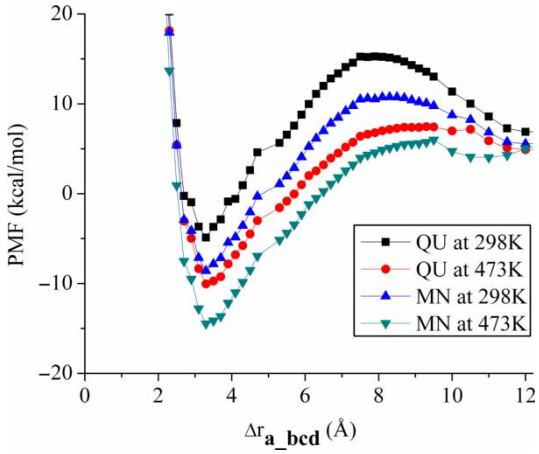

Figure 5. PMF plots for Maya asphaltene disaggregation in quinoline (QU) and 1-methylnaphthalene (MN) at 298 and 473 K in NVT, obtained for geometry optimisation with a constraint (described in the text). Charges are obtained using the Hirshfeld population analysis. The Maya asphaltene geometry is optimised using Harris/DN/DMol^3.

Table 1. The aggregation PMF (kcal/mol) of Maya asphaltene in quinoline (QU) and 1-methylnaphthalene (MN) solvents at 298 and 473 K. The charges are from separate molecule (single point for total aggregate) calculation.

				a_bcd			abc_d		
Solvent	Charges	T	Density	PMF_{max}	PMF_{min}	$PMF_{max} - PMF_{min}$	PMF_{max}	PMF_{min}	$PMF_{max} - PMF_{min}$
Disaggregation I									
QU	Hirshfeld	298	1.09	15.96 (16.11)	− 11.06 (− 11.84)	27.02 (27.95)	19.67 (20.26)	− 16.89 (17.93)	36.56 (38.19)
		473	0.95	5.13 (5.37)	− 19.53 (− 20.26)	24.66 (25.63)	6.25 (6.97)	− 25.19 (− 26.03)	31.44 (33.00)
	Mulliken	298	1.09	17.54 (17.48)	− 0.79 (− 1.71)	18.33 (19.19)	21.61 (21.33)	− 8.75 (− 12.23)	30.36 (33.56)
		473	0.95	6.48 (7.14)	− 9.75 (− 10.63)	16.23 (17.77)	8.76 (8.77)	− 17.98 (− 21.05)	26.74 (29.82)
MN	Hirshfeld	298	1.02	10.19 (10.11)	− 14.20 (− 16.67)	24.39 (26.78)	13.21 (13.17)	− 19.28 (− 22.51)	32.49 (35.68)
		473	0.94	2.75 (2.67)	− 22.02 (− 24.45)	24.77 (27.12)	3.96 (3.98)	− 27.24 (− 30.46)	31.20 (34.44)
	Mulliken	298	1.02	11.82 (11.91)	− 5.72 (− 6.61)	17.54 (18.52)	14.12 (14.26)	− 14.15 (− 17.19)	28.27 (31.45)
		473	0.94	6.48 (4.65)	− 14.33 (− 15.22)	20.81 (19.87)	5.41 (5.34)	− 23.46 (− 26.45)	28.87 (31.79)
Disaggregation II									
QU	Hirshfeld	298	1.09	11.07	− 5.38	16.45	12.08	− 19.70	31.78
		473	0.95	0.31	− 12.63	12.94	− 0.24	29.13	28.89
MN	Hirshfeld	298	1.02	5.20	− 9.77	14.97	4.47	− 25.19	29.68
		473	0.94	− 2.62	− 16.94	14.32	− 3.19	− 33.63	30.44

aggregation preferences might be predictable by using Fukui functions and reactivity indices [16].

The PMFs resulting from the disaggregation path followed are shown in Figure 5. These PMF plots are not as smooth as those obtained without geometry optimisation, because along the path the structures cross between different paths, and the probability of path crossing increases at high temperatures. The broad peak maxima arise from the gradual disaggregation, as opposed to the abrupt disaggregation for configurations I and II. The PMF barrier for disaggregation in quinoline decreases from 20.16 to 17.52 kcal/mol for the temperature rise from 298 to 473 K. On the contrary, in methylnaphthalene it increases from 19.34 to 20.37 kcal/mol for the same temperature rise.

In Figure 6, we show the statistical solvent distribution upon AS–MY disaggregation. This allows us to predict the most probable solvent molecule distribution. For example, the H_1 and N atoms are distributed close to the asphaltene π–conjugated system, suggesting that the quinoline molecule could undergo $\pi-\pi$ interaction with the aromatic asphaltene moieties that would compete with the aggregation among the asphaltene molecules. Controlling the strength of such interaction and its evolution with temperature and density might be crucial for disaggregation. In Figure 6(b) and (c), we show that upon disaggregation, quinoline solvent molecules enter into the space between the disaggregated asphaltene units at the distances higher than the PMF_{max} values shown in Figure 4.

4. Conclusion

Asphaltene disaggregation is a slow process that involves soaking and heating in organic solvents. The main advantage of the 3D-RISM statistical approach compared with the molecular simulations we applied is that the theory works at an ensemble of solvent configurations in the entire phase space, giving access to processes that occur on large space and time scale. The initial structure and atomic charges of Maya asphaltene are calculated using the Harris approximation, as implemented in DMol^3. For the three disaggregation pathways investigated, we found that Maya asphaltene disaggregation in quinoline increases at 473 K, compared with 298 K. However, this effect is not observed in 1-methylnaphthalene. The PMF barrier changes obtained for the different disaggregation modes show the importance of disaggregation path crossing. The method of disaggregation path following the one which we applied becomes unrealistic at high temperature due to the increasing probability of path crossing.

The Hirshfeld charges yield higher $PMF_{max} - PMF_{min}$ values than the Mulliken charges in quinoline, while not affecting the respective values in 1-methylnaphthalene. Our theoretical model predicts the solvent distribution and the PMF, which is related to the aggregate stability in the

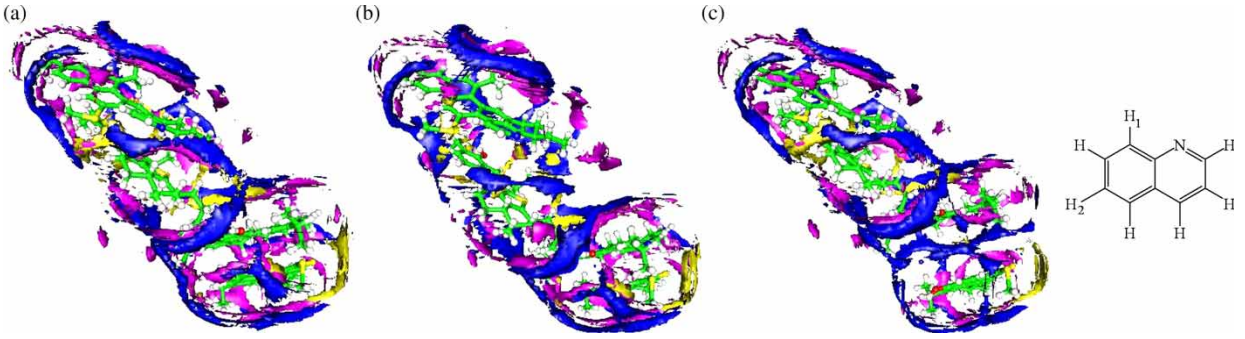

Figure 6. Quinoline solvent molecules enter between Maya asphaltene molecules upon disaggregation at 298 K. (a) The optimised geometry. In (b) and (c), the Δr_{a_bcd} and Δr_{abc_d} are 6.7 and 6.0 Å, respectively. The solvent distribution functions of the quinoline atoms N ($g = 2.2$), H_1 ($g = 1.4$) and H_2 ($g = 1.6$) are shown in blue, purple and yellow, respectively.

external conditions investigated, such as temperature and solvent density. Compared with MD, our statistical approach is much less expensive and provides access to large-scale and slow solvation processes by probing the entire phase space. It readily allows one to model supramolecular aggregation and reactions in solvents and mixtures of given thermodynamic conditions and compositions, including viscous and complex liquids.

We chose the analysis of PMF for a given pathway of disaggregation to illustrate the effect of two solvents of different polarities and chemical specificities, heterocyclic (quinoline) and hydrocarbon (methylnaphthalene), on the disaggregation. A complete study would involve QM/MD/3D-RISM-type calculations with 3D-RISM contracting solvent degrees of freedom and MD applied to conformations of asphaltene to explore its entire phase space and find the optimal pathway of disaggregation. We postpone this analysis for future implementations coupling 3D-RISM with QM/MD in one of the computational chemistry packages.

Acknowledgements

This work was supported by the National Institute for Nanotechnology, National Research Council of Canada. The computations were performed at the Centre of Excellence in Integrated Nanotools (CEIN) at the University of Alberta.

References

[1] F. Ding, S.H. Ng, C. Xu, and S. Yui, *Reduction of light cycle oil in catalytic cracking of bitumen-derived crude HGOs through catalyst selection*, Fuel Proc. Technol. 88 (2007), pp. 833–845.

[2] J. Murgich, J.M. Rodrigues, and Y. Aray, *Molecular recognition and molecular mechanics of micelles of some model asphaltenes and resins*, Energy Fuels 10 (1996), pp. 68–76.

[3] E. Rogel, *Studies on asphaltenes aggregation via computational chemistry*, Colloids Surf. A 104 (1995), pp. 85–93.

[4] T. Takanohashi, M. Iino, and K. Nakamura, *Evaluation of association of solvent-soluble molecules of bituminous coal by computer simulation*, Energy Fuels 8 (1994), pp. 395–398; T. Takanohashi, M. Iino, K. Nakamura, *Simulation of interaction of coal associates with solvents using the molecular dynamics calculation*, Energy Fuels 12 (1998), pp. 1168–1173.

[5] T. Takanohashi, S. Sato, I. Saito, and R. Tanaka, *Molecular dynamics simulation of the heat-induced relaxation of asphaltene aggregates*, Energy Fuels 8 (2003), pp. 135–139.

[6] T. Takanohashi, S. Sato, and R. Tanaka, *Molecular dynamics simulation of structural relaxation of asphaltene aggregates*, Petr. Sci. Technol. 21 (2003), pp. 491–505.

[7] T. Takanohashi, S. Sato, and R. Tanaka, *Structural relaxation behaviors of three different asphaltenes using MD calculations*, Petr. Sci. Technol. 22 (2004), pp. 901–914.

[8] D. Scott, D. Radlein, J. Piskorz, P. Majerski, and T.J.W. deBruijn, *Upgrading of bitumen in supercritical fluids*, Fuel 80 (2001), pp. 1087–1099.

[9] A. Kovalenko, *Three-dimensional RISM theory for molecular liquids and solid–liquid interfaces*, in *Understanding Chemical Reactivity: Molecular Theory of Solvation*, F. Hirata ed., Vol. 24, Kluwer Academic Publishers, New York, NY, 2003, pp. 169–275.

[10] S. Gusarov, T. Ziegler, and A. Kovalenko, *Self-consistent combination of the three-dimensional RISM theory of molecular solvation with analytical gradients and the amsterdam density functional package*, Phys. Chem. A 110 (2006), pp. 6083–6090.

[11] D. Casanova, S. Gusarov, A. Kovalenko, and T. Ziegler, *Evaluation of the SCF combination of KS-DFT and 3D-RISM–KH; solvation effect on conformational equilibria, tautomerization energies, and activation barriers*, J. Chem. Theory. Comput. 3 (2007), pp. 458–476.

[12] A. Kovalenko and F. Hirata, *Self-consistent description of a metal-water interface by the Kohn–Sham density functional theory and the three-dimensional reference interaction site model*, J. Chem. Phys. 110 (1999), pp. 10095–10112.

[13] A. Kovalenko and F. Hirata, *Towards a molecular theory for the Van der Walls–Maxwell description of fluid phase transitions*, J. Theor. Comput. Chem. 1 (2002), pp. 381–406.

[14] A. Kovalenko and F. Hirata, *First-principles realization of a Van der Waals–Maxwell theory for water*, Chem. Phys. Lett. 349 (2001), pp. 496–502.

[15] S.R. Stoyanov, P. Král, and B. Wang, *Extended electronic states above metal-doped carbon nanostructures*, Appl. Phys. Lett. 90 (2007), pp. 153110-1–153110-3.

[16] S.R. Stoyanov, S. Gusarov, S.M. Kuznicki, and A. Kovalenko, *Theoretical modeling of zeolite nanoparticle surface acidity for heavy oil upgrading*, J. Phys. Chem. C 112 (2008), pp. 6794–6810.

[17] *DMol*^{3}, *Release 4.0*, Accelrys, Inc., CA (2001)

[18] J. Harris, *Simplified method for calculating the energy of weakly interacting fragments*, Phys. Rev. B 31 (1985), pp. 1770–1779.

[19] S.J. Vosko, L. Wilk, and M. Nusair, *Accurate spin-dependent electron liquid correlation energies for local spin density calculations: A critical analysis*, Can. J. Phys. 58 (1980), pp. 1200–1211.

[20] B. Delley, *An all-electron numerical method for solving the local density functional for polyatomic molecules*, J. Chem. Phys. 92 (1990), pp. 508–517.
[21] F.L. Hirshfeld, *Bonded-atom fragments for describing molecular charge densities*, Theor. Chim. Acta B 44 (1977), pp. 129–138.
[22] R.S. Mulliken, *Electronic population analysis on LCAO–MO [linear combination of atomic orbital–molecular orbital] molecular wave functions. I.; Electronic population analysis on LCAO–MO [linear combination of atomic orbital-molecular orbital] molecular wave functions. II. Overlap populations, bond orders, and covalent bond energies*, J. Chem. Phys. 23 (1955), pp. 1833–1846.
[23] M. Freindorf and J. Gao, *Optimization of the Lennard-Jones Parameters for a combined* ab initio *quantum mechanical and molecular mechanical potential using the 3-21G basis set*, J. Comput. Chem. 17 (1996), pp. 386–395.
[24] W. Jorgensen and J. Tirado-Rives, *The OPLS potential functions for proteins. Energy minimizations for crystals of cyclic peptides and crambin*, J. Am. Chem. Soc. 110 (1988), pp. 1657–1666.
[25] J.P. Perdew and Y. Wang, *Pair-distribution function and its coupling-constant average for the spin-polarized electron gas*, Phys. Rev. B 45 (1992), pp. 13244–13249.
[26] F. Alvarez-Ramirez, E. Ramirez-Jaramillo, and Y. Ruiz-Moralez, *Calculation of the interaction potential curve between asphaltene-asphaltene, asphaltene-resin, and resin-resin systems using density functional theory*, Energy Fuels 20 (2006), pp. 195–204.